Pergamon

Int. J. Heat Mass Transfer. Vol. 39, No. 13, pp. 2663–2670, 1996

0017–9310/96 $15.00+0.00

0017–9310(95)00366–5

Natural convection of high Prandtl number fluids with variable viscosity in a vertical slot

Y. Y. JIN and C. F. CHEN†

Department of Aerospace and Mechanical Engineering, The University of Arizona, Tucson, AZ 85721, U.S.A.

(*Received* 1 *May* 1995 *and in final form* 5 *October* 1995)

Abstract—Natural convection of high Prandtl number fluids with temperature-dependent viscosity in a vertical slot with aspect ratio 15 is studied numerically. A four-parameter fit for the variable viscosity is adopted. The flow patterns and the critical Grashof numbers predicted are in good agreement with earlier experimental results of Chen and Thangam [*J. Fluid Mech.* **161,** 161–173 (1985)]. The critical Grashof number is lower than the corresponding value obtained for the constant viscosity fluid, and it varies almost inversely with the Prandtl number. The viscosity stratification and the large vertical temperature gradient in the lower region of the slot cause the secondary cells to appear in the upper region of the central core at onset. The heat transfer rate is slightly smaller than that in constant property case as the viscosity variation becomes large. Copyright © 1996 Elsevier Science Ltd.

1. INTRODUCTION

By a series of experiments using high-Prandtl-number fluids, Elder [1] discovered the abrupt transition from a unicellular convective flow pattern into a steady secondary flow pattern that occurs when the lateral temperature difference across a vertical slot, or non-dimensionally the Rayleigh number, exceeds the critical value. The secondary flow consists of a vertical array of convection cells. At still higher Rayleigh numbers, a tertiary flow pattern emerges in which small counter-rotating cells are observed sandwiched between the well-established secondary cells. This discovery prompted a series of research efforts on this interesting phenomenon. Vest and Arpaci [2] considered the stability of convection in a vertical slot of infinite height. They applied the linear stability analysis to two different basic states. One was the conduction state in which the temperature gradient was uniform across the slot, and the other was the boundary layer state in which a finite vertical temperature gradient was imposed on the slot. Hart [3] performed experiments and linear stability analyses on the convection flow generated in air and in water contained in a differentially heated tall cavity that was inclined from the vertical. The linear stability analysis was made on the boundary layer state with the experimentally determined vertical temperature gradient. Good agreement was obtained between the experimental and theoretical results.

Lee and Korpela [4] conducted extensive numerical computations of the problem based on the nonlinear governing equations for a constant-property fluid with the Boussinesq assumption. Calculations were made for liquid metal, air, and water. Results clearly showed the onset of secondary flow as the critical Rayleigh number was exceeded, and further intensification of convection as the Rayleigh number was increased. In the case of water, they found the existence of travelling waves, as predicted and observed by Hart [3].

Chen and Thangam [5] carried out experiments with glycerine–water solutions of 70, 80 and 90% glycerine. The Prandtl numbers of these solutions evaluated at the mean temperature were 158, 405 and 720, respectively. The corresponding ratios of kinematic viscosities evaluated at the temperatures of the cold and hot walls at the critical state were 2.15, 6.70 and 27.20. They determined experimentally the critical Rayleigh numbers for the onset of secondary flow and recorded the flow by shadowgraph at supercritical states. They also calculated the critical Rayleigh number by linear stability analysis based on the conduction state. These values were found to be approximately half of the experimental values because the stability effect of the vertical temperature gradient was not accounted for. Later, Thangam and Chen [6] carried out a stability analysis throughout the Prandtl number range for a variable viscosity fluid with different values of the exponential viscosity parameters. Chen and Pearlstein [7] carried out a linear stability analysis of variable-viscosity fluids in vertical and inclined slots. They used a four-parameter viscosity model [8] that reproduced very accurately the measured viscosity of the glycerine–water solution. Their results for the vertical slot differed from those of Thangam and Chen [6] not only because of the difference in the viscosity models used but also in the number of terms in the Galerkin expansion. Apparently, the number of terms used by Thangam and Chen [6] was not sufficient

† Author to whom correspondence should be addressed.

NOMENCLATURE

A	aspect ratio, H/L
C	glycerine concentration in aqueous solution
D, E, F, G	parameters of viscosity correlation
f	dynamic viscosity ratio, $\mu(T)/\mu_m$
g	gravitational acceleration
Gr	Grashof number, $g\beta_m\Delta TL^3/\nu_m^2$
H	height of the slot
J	Jacobian derivative, $J(\omega,\psi) = \partial\psi/\partial y\,\partial\omega/\partial x - \partial\psi/\partial x\,\partial\omega/\partial y$
L	width of the slot
Nu	Nusselt number
Pr	Prandtl number, ν_m/α_m
Ra	Rayleigh number, $g\beta_m\Delta TL^3/\alpha_m\nu_m$
S	dimensionless vertical temperature gradient at the center, $\partial\theta/\partial y$
t	dimensionless time
T	temperature
x, y	dimensionless Cartesian coordinates
U	characteristic velocity, $g\beta_m\Delta TL^2/\nu_m$
u, v	dimensionless velocity components.

Greek symbols

α	thermal diffusivity
β	coefficient of volumetric expansion
ΔT	temperature difference
θ	dimensionless temperature
μ	dynamic viscosity
ν	kinematic viscosity
ρ	density
ψ	stream function
ω	vorticity
∇^2	del operator, $\partial^2/\partial x^2 + \partial^2/A^2\partial y^2$.

Subscripts

c	cold wall or critical value
h	hot wall
L	local value
m	value at the mean temperature of the vertical walls
max	maximum value.

for convergence. But the predicted critical Rayleigh numbers reported by Chen and Pearlstein were still much lower than the experimental values of Chen and Thangam [5].

Seki *et al.* [9] carried out experiments with fluids whose Prandtl number varied from 4 to 12 500 in a tall vertical cavity whose aspect ratio varied from 6 to 30. They also obtained numerical solutions based on the assumption of constant property. Their interest was mainly in the heat transfer characteristics over a large range of Rayleigh numbers up to 10^{11}. In their flow visualization studies, they noted that in glycerine the onset of secondary flow first occurred in the upper portion of the slot. More recently, Chen and Wu [10] made a careful experimental study of the flow process at supercritical states beyond the tertiary flow regime using the much more sensitive Schlieren technique. Wakitani [11] carried out experiments with silicone oils with Prandtl numbers up to 900. Flow visualization studies were carried out using particle traces.

In this paper, we report the results of numerical calculations, focusing our attention on the transition process for the experimental cases studied by Chen and Thangam [5]. The governing equations, the numerical methods, and the viscosity model used are described in Section 2. An accuracy assessment of the code is presented in Section 3. The results of the calculations are presented and discussed in Section 4 and summarized in Section 5.

2. GOVERNING EQUATIONS AND NUMERICAL ALGORITHM

2.1. *Governing equations*

A Newtonian fluid with constant properties except the dynamic viscosity μ, which is a function of temperature, is contained in a vertical slot of height H and width L. The horizontal walls of the slot are impermeable and adiabatic. Its left and right walls are maintained at uniform constant temperatures, T_h and T_c ($< T_h$), respectively. A convective flow is then generated by the lateral temperature difference, which is assumed to be small enough so that the Boussinesq approximation holds. The governing equations describing the flow can be nondimensionalized by scaling the vertical coordinate by H, the horizontal coordinate by L, time by L^2/ν_m, temperature by $\Delta T = T_h - T_c$, velocity by $U = g\beta_m\Delta TL^2/\nu_m$, and pressure by $\rho_m U^2$. Here, the kinematic viscosity ν_m is evaluated at the mean temperature of the vertical walls. Introducing the stream function ψ and vorticity ω

$$u = \frac{1}{A}\frac{\partial\psi}{\partial y} \quad v = -\frac{\partial\psi}{\partial x} \tag{1}$$

$$\omega = \frac{\partial v}{\partial x} - \frac{1}{A}\frac{\partial u}{\partial y} \tag{2}$$

we obtain the nondimensional governing equations:

$$\frac{\partial \omega}{\partial t} = -\frac{Gr}{A} J(\omega, \psi) + f\nabla^2\omega + \frac{\partial \theta}{\partial x} + 2\left(\frac{\partial f}{\partial x}\frac{\partial \omega}{\partial x} + \frac{\partial f}{A\,\partial y}\frac{\partial \omega}{A\,\partial y}\right) - \left(\frac{\partial^2 \psi}{\partial x^2} - \frac{\partial^2 \psi}{A^2\,\partial y^2}\right)\left(\frac{\partial^2 f}{\partial x^2} - \frac{\partial^2 f}{A^2\,\partial y^2}\right) - 4\frac{\partial^2 f}{A\,\partial x\,\partial y}\frac{\partial^2 \psi}{A\,\partial x\,\partial y} \quad (3)$$

$$\nabla^2\psi = -\omega \quad (4)$$

$$\frac{\partial \theta}{\partial t} = -\frac{Gr}{A} J(\theta, \psi) + \frac{1}{Pr}\nabla^2\theta \quad (5)$$

where $f = \mu(T)/\mu_m$ is the dynamic viscosity ratio. The physical properties except the dynamic viscosity $\mu(T)$ in the above equations are determined at the mean temperature. The boundary conditions are

$$x = 0 \quad \psi = \partial\psi/\partial x = 0 \quad \theta = 1 \quad (6)$$

$$x = 1 \quad \psi = \partial\psi/\partial x = 0 \quad \theta = 0 \quad (7)$$

$$y = 0 \quad \psi = \partial\psi/\partial y = 0 \quad \partial\theta/\partial y = 0 \quad (8)$$

$$y = 1 \quad \psi = \partial\psi/\partial y = 0 \quad \partial\theta/\partial y = 0. \quad (9)$$

A finite difference method suggested by Lee and Korpela [4] is used to solve the above governing equations. It consists of the explicit method of Arakawa [12] for the nonlinear terms, the DuFort–Frankel [12] method for the diffusive terms, and the central difference scheme for the time derivatives to discretize the equations. The Poisson equation [4] is solved by the Alternating Direction Implicit (ADI) method [12], aided with the prediction method [13] and Block Correction Technique (BCT) [14]. The boundary vorticity is determined by Thom's rule [12]. Calculations at the specific Prandtl numbers are started from an initially motionless state. Calculations at the higher Grashof numbers are then initiated from the results of lower Grashof numbers.

2.2. *Viscosity variations of the glycerine–water solution*

Calculations have been made for 70, 80 and 90% glycerine–water solutions, which were used in the experiments by Chen and Thangam [5]. Following Chen and Pearlstein [7], we use a four-parameter expression for μ:

$$\mu(T) = D\exp(E/T^3 + FT + G/T) \quad (10)$$

where T is the absolute temperature, D, E, F and G are four parameters given by Chen and Pearlstein [8]. This four-parameter form gives a very accurate correlation to the variable viscosity of the aqueous glycerol solution.

During the simulation, the reference temperature is fixed at the mean value of the vertical wall temperatures given in experiment by Chen and Thangam [5], that is, $T_m = 22.4°C$, 22.7°C and 33.4°C for $C = 70$, 80 and 90% glycerine–water solutions, respectively. The physical properties except the density and variable viscosity given in their report are used to define the Prandtl and Grashof numbers. The Prandtl numbers at these reference temperatures are 158, 405 and 720 for $C = 70$, 80 and 90%, respectively.

3. ACCURACY ASSESSMENT

The code based on the above algorithm has been tested by calculating the natural convection of air in vertical slots with aspect ratio $A = 16$ and 20, and comparing with known results. Detailed comparison can be found in Jin and Chen [15]. The following is a brief summary.

For $A = 16$, we compared our results with those of the two-cell solution at $Ra = 24\,000$ ($Gr = 33\,803$) calculated by Le Quéré [16] using Tau–Chebyshev algorithm. A grid convergence study showed that a 33×129 grid gave satisfactory results, within 3% of those of Le Quéré for the most sensitive quantity, the vorticity in the slot. The streamlines showed a two-cell secondary flow pattern with a wavenumber approximately 1.60 [15]. The flow pattern and the wavenumber were in good agreement with the results by Le Quéré [16], who obtained a wavenumber 1.59.

For $A = 20$, we obtained the critical Grashof number $Gr_c = 8800$–8900, which was in excellent agreement with that predicted by Lauriat and Desrayaud [17], who obtained $Gr_c = 8900$.

4. RESULTS AND DISCUSSION

4.1. *Flow development at* C = 80%

Results with $C = 80\%$ are presented in detail and compared with the available experiments in this section. Convective streamline patterns in the cavity as Gr is increased from 50 to 2000 are shown in Fig. 1. A unicellular flow is generated by the lateral temperature difference at $Gr = 50$ as shown in Fig. 1(a), the flow is symmetric except at the two ends as in the case of constant viscosity, high Prandtl number fluid because of the small viscosity variation in the slot. The flow enters the boundary layer regime very soon as the Grashof number is increased. At $Gr = 800$ ($\Delta T = 30.2°C$), Fig. 1(b), the boundary layer structure is clearly exhibited with the boundary layer along the right cold wall slightly thicker than that along the left hot wall because of the difference in viscosity. A slight increase of Grashof number to 850 ($\Delta T = 32.1°C$), Fig. 1(c), triggers the onset of convective instability, with three small secondary cells rotating in the same direction as the originally unicellular flow. These cells have an averaged wavelength of $1.60L$ or wavenumber of 3.92, which is larger than that obtained in the experiments of Chen and Thangam [5], who gave the critical wavenumber 3.1. These secondary cells, sloping down from the hot wall to the cold, are located in the upper part of the central core.

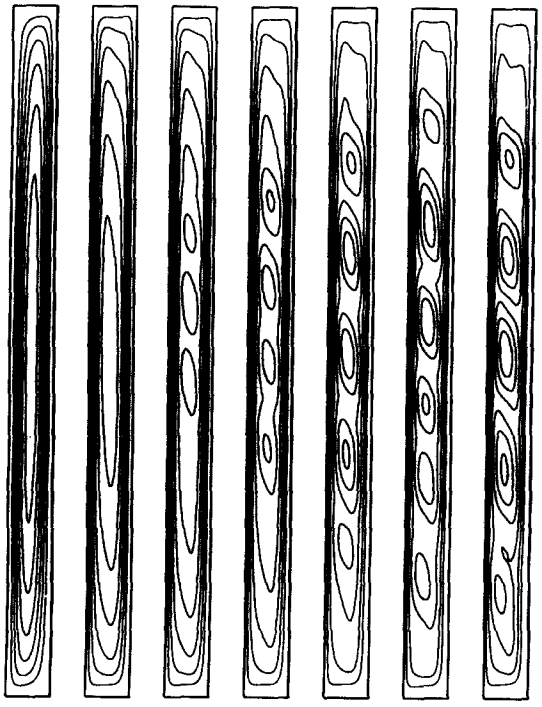

Fig. 1. Typical flow patters at 80% glycerine–water solution: (a) $Gr = 50$, $\psi = -28$, -56, -84, -112, -140 and -168×10^{-5}; (b) $Gr = 800$, $\psi = -6$, -12, -18, -24, -30 and -35×10^{-5}; (c) $Gr = 850$, $\psi = -6$, -12, -18, -24, -30 and -36×10^{-5}; (d) $Gr = 1000$, $\psi = -6$, -12, -18, -24, -30 and -35×10^{-5}; (e) $Gr = 1200$, $\psi = -6$, -12, -19, -25, -30 and -34×10^{-5}; (f) $Gr = 1500$, $\psi = -5$, -10, -16, -22, -27 and -31×10^{-5}; (g) $Gr = 2000$, $\psi = -5$, -10, -15, -20, -25 and -29×10^{-5}.

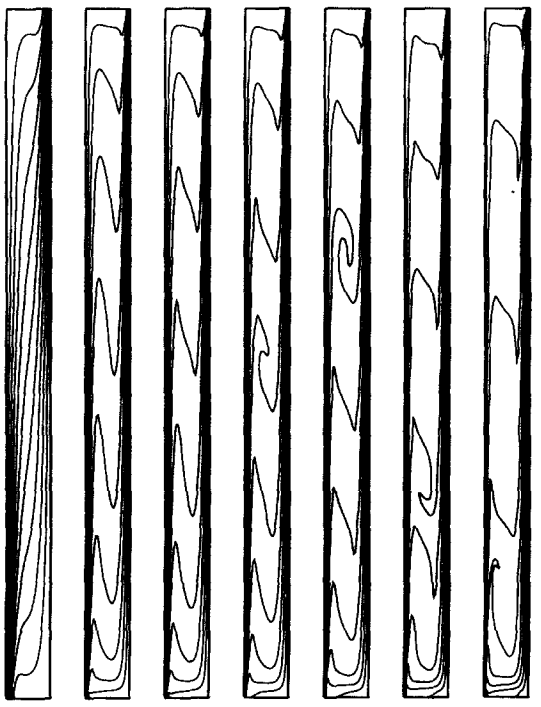

Fig. 2. Isotherms at 80% glycerine–water solution: (a) $Gr = 50$; (b) $Gr = 800$; (c) $Gr = 850$; (d) $Gr = 1000$; (e) $Gr = 1200$; (f) $Gr = 1500$; (g) $Gr = 2000$.

This upward displacement of the secondary cells, which was clearly observed in the experiment of Seki *et al.* [9] is due to the viscosity variation. At this time, the ratio of fluid viscosity, ν_c/ν_h, at the cold and hot walls reaches 6.77. When the Grashof number is increased to 1000 ($\Delta T = 37.8°C$), four secondary cells are developed [Fig. 1(d)]. The cell at the top is more vigorous while the cells in the lower part are weaker. More cells are generated when the Grashof number is increased. Five cells are found at $Gr = 1200$ ($\Delta T = 45.3°C$) as shown in Fig. 1(e). At this ΔT, the average wavenumber is 3.03. This wavenumber is now very close to the experimental result given by Chen and Thangam [5]. In their experiment, Chen and Thangam [5] observed three secondary cells at $\Delta T = 33°C$, four cells at $\Delta T = 35.3°C$, and five cells at $\Delta T = 45°C$, respectively. These temperature differences correspond approximately to Grashof numbers $Gr = 873$, 934 and 1191, respectively, very close to the cases shown in Figs 1(c)–(e). The predicted flow patterns are qualitatively in good agreement with the observation in the experiments.

As the Grashof number is increased to 1500, Fig. 1(f), one more secondary cell is generated in the cavity. The cells in the upper region of the central core are more vigorous than those in the lower part because of smaller viscosity due to higher temperature. When the Grashof number is increased to 2000, Fig. 1(g), five secondary cells remain because of merging. The temperature difference between the vertical walls reaches 75.5°C, and the viscosity ratio $\nu_c/\nu_h = 119.5$, beyond the experimental range of Chen and Thangam [5]. The flow along the left wall is confined to a layer much thinner than that on the right side. The secondary cells are pushed towards the left wall, as clearly observed in the experiments by Chen and Thangam [5].

The corresponding isotherms are shown in Fig. 2. At $Gr = 50$ [Fig. 2(a)], a stable temperature gradient, which is typical in the transition regime, is established in the core region indicating the effect of convection although the Grashof number is very small. The flow enters the boundary layer regime, which is clearly exhibited by the isotherms, at $Gr = 800$ as shown in Fig. 2(b), with convection becoming the predominant heat transfer mode in the slot. The thermal boundary layer along the right wall is thicker than that along the left wall. The isotherms indicate a larger vertical temperature gradient at the bottom of the cavity. At $Gr = 850$, Fig. 2(c), secondary cellular flow has developed in the central core of the cavity as indicated by the streamline patterns [Fig. 1(c)], but because of the weak circulation, the isotherms are hardly distorted. The streamlines also indicate the secondary cells are in the upper half of the cavity. This is due to:

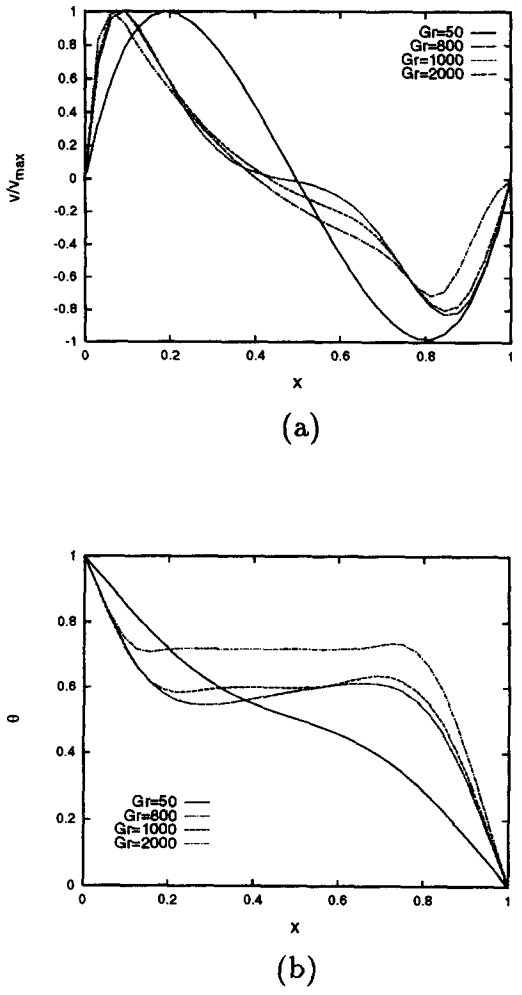

Fig. 3. Reduced vertical velocity and horizontal temperature profiles at the middle height: (a) velocity; (b) temperature.

(i) the smaller viscosity in the top portion of the cavity because of the stable vertical temperature gradient and (ii) the larger temperature gradient in the bottom, which has a stabilizing effect on the flow. When the Grashof number is increased, the secondary cellular flow becomes stronger, causing even larger distortions in the isotherms as shown in Figs 2(d)–(g). A notable difference can be found by comparing the boundary layer at the lower right corner with that at upper left corner. The isolines at the bottom become denser, which imply the strong variation in temperature, and result in large variation in the viscosity of the fluid. The isolines of the temperature move down with increasing Grashof number. The distance between two isolines in the vertical direction of the main region is enlarged, which indicates a decrease in temperature gradient, due to the strong mixing of the fluid in the main region.

The reduced vertical velocity v/v_{max} and the horizontal temperature distribution at the mid-height are shown in Fig. 3 with $v_{max} = 5.91$, 1.79, 1.68 and 1.52×10^{-3} for $Gr = 50$, 800, 1000 and 2000, respectively. At $Gr = 50$, the reduced vertical velocity, Fig. 3(a), is nearly odd-symmetric. When the Grashof number is increased, the symmetry disappears as shown at $Gr = 800$. The negative peak values become progressively smaller than the positive peaks as Gr is increased. At the same time, both the positive and the negative peak zones move further to the left, indicating the thinning of upward boundary layer and thickening of the downward boundary layer due to viscosity variation. In addition, the difference between the two peak values increases with the Grashof number, which confirms the more evident effect of the variable viscosity on the flow.

The temperature profile at $Gr = 50$, Fig. 3(b), shows a relatively minor distortion from the conduction profile. At $Gr = 800$, the boundary layer structure is clearly reflected in the temperature profile. The temperature in the core region shows a reverse horizontal gradient, similar to that found in constant property fluids as obtained in experiment by Elder [1] and Wakitani [11]. At $Gr = 1000$, strong convective mixing in the core raises the temperature of the fluid close to the hot wall and causes the disappearance of the reverse temperature gradient. This latter feature is quite different from the case of constant property fluid, in which a notable reverse temperature gradient, largest at the mid-height, exists even at high value of Gr as indicated by Elder [1] and Wakitani [11].

Typical profiles of the horizontal velocity, and temperature along the vertical central line are shown in Fig. 4 for $Gr = 800$, 850 and 1500. Before the appearance of the secondary cellular flow, the velocity already shows very small waviness at around the mid-height of the slot as shown in Fig. 4(a) at $Gr = 800$. At $Gr = 850$, large waviness of the horizontal velocity is developed, corresponding the visible secondary cells in Fig. 1(c). The amplitude of the horizontal velocity variations is slightly larger in the upper region than in the lower part, which indicates a stronger convective motion in the upper due to the viscosity decrease. This feature is more evident when the Grashof number is increased as shown at $Gr = 1500$. The wave-like variations of the vorticity and stream function are similar as the horizontal velocity.

The temperature profile along the vertical centerline as shown in Fig. 4(b). Before the onset of the convective instability, the temperature increases smoothly from the bottom to the top of the cavity at $Gr = 800$. The positive temperature gradient in the lower region is larger than that in the upper. A small disturbance in temperature is discernible at the center point. When the secondary cellular flow sets in, the temperature profile shows a wavelike variation, with a step change of temperature between the secondary cells. The temperature within the secondary zone varies slightly, and shows a reverse vertical gradient with higher temperature at the low part. As the Grashof number is increased, the reverse temperature gradient decreases because of the strong mixing within the cell as shown at $Gr = 1500$. The entire profile at $Gr = 1500$ moves

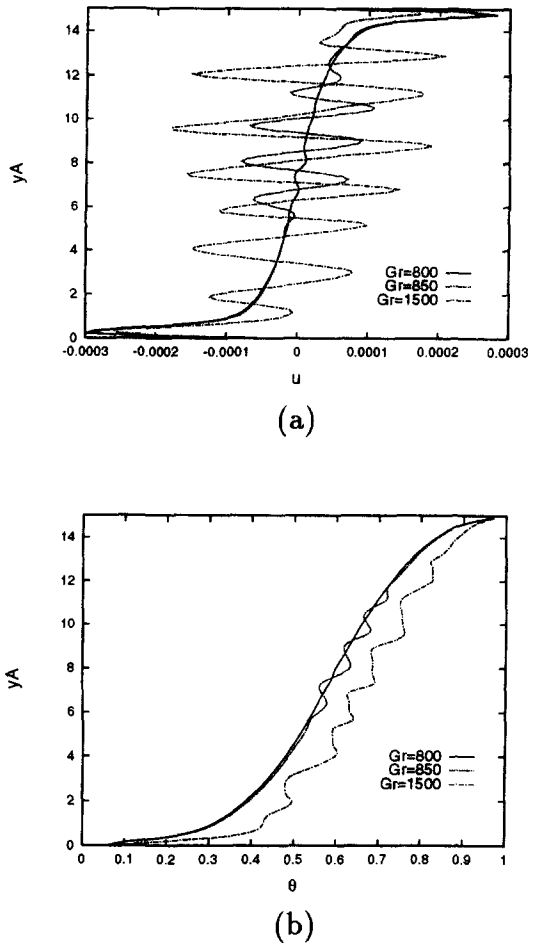

Fig. 4. Typical profiles of the horizontal velocity and temperature alone the vertical center line (a) velocity; (b) temperature.

to the right, indicating a significant increase of the fluid temperature. This feature is in accord with the flow pattern shown in Fig. 1(f). At $Gr = 1500$, the upward boundary layer along the left hot wall is very thin. The secondary cells are notably pushed towards the left wall. Therefore the temperature in the cells is increased, and the temperature at the center line is also increased due to the strong convection within the cells.

The flow developments at $C = 70\%$ and 90% are similar to the case of $C = 80\%$. Only the flow patterns around the onset of the secondary cellular flow in case of $C = 90\%$ are given here for comparison with the experimental observation by Chen and Thangam [5]. The flow is unicellular at $Gr = 450$ ($\Delta T = 47.9°C$) as shown in Fig. 5(a). At $Gr = 500$ ($\Delta T = 53.3°C$), there are four visible secondary cells with an average wavenumber 3.62 as shown in Fig. 5(b). Chen and Thangam [5] observed four secondary cells at $\Delta T = 55.8°C$ ($Gr = 524$), with a wavenumber 3.4. The current prediction is in good agreement with their experimental results.

Fig. 5. Typical flow patterns at 90% glycerine–water solution with $\psi = -6, -12, -18, -24, -30$ and -36×10^{-5}: (a) $Gr = 450$; (b) $Gr = 500$.

4.2. *Critical Grashof number*

The critical Grashof number at the onset of the secondary cellular flow is shown in Table 1 and Fig. 6 with the available experimental and analytical results. The predicted values are in good agreement with the experiment of Chen and Thangam [5], but much higher than the analytical results by Chen and Thangam [5] and Chen and Pearlstein [7], as shown in Fig. 6. The critical Grashof number data suggest a correlation of the following form

$$Gr_c = 4.96 \times 10^5 Pr^{-1.06} \tag{11}$$

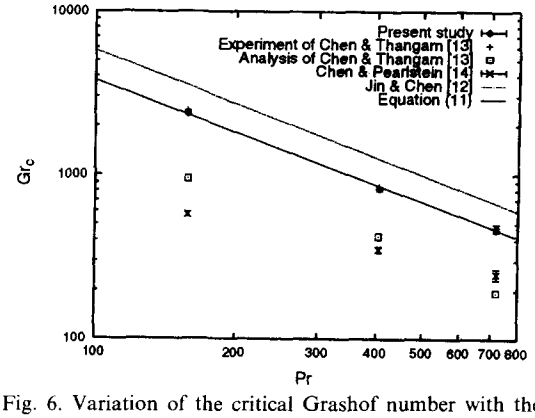

Fig. 6. Variation of the critical Grashof number with the Prandtl number. Note results of present study, and Chen and Pearlstein [7] are plotted with error bars.

Table 1. Critical values at the onset of the secondary flow compared with available experimental and analytical results

	70%	80%	90%	Authors
Gr_c	2300–2400	800–850	450–500	Present study
	2456	844	461	Chen and Thangam [5], experiment
	944	422	194	Chen and Thangam [5], analysis
	588	365	269	Chen and Pearlstein [7]
	550	336	232	Chen and Pearlstein [7]
	3300–3500	1200–1300	700–720	Jin and Chen [15], constant property
S_1	0.388	0.328	0.304	Present study
	0.315	0.315	0.315	Chen and Thangam [5], experiment
S_2	0.479	0.463	0.430	Present study
	0.491	0.474	0.443	Estimated by equation (12) [1]
ν_h/ν_m	0.697	0.434	0.259	Present study
ν_c/ν_h	2.16	6.77	29.5	Present study
k_c	3.92	3.86	3.62	Present study
	3.1	2.9	3.4	Chen and Thangam [5], experiment
	2.39	2.46	2.24	Chen and Thangam [5], analysis
	2.48	2.40	2.26	Chen and Pearlstein [7]
	2.36	2.21	2.06	Chen and Pearlstein [7]

with a maximum deviation 3.6% at $C = 80\%$. This correlation is also shown in the same figure. The critical values obtained for the corresponding constant viscosity fluids by Jin and Chen [15] are shown in Fig. 6 for comparison. The two results are nearly parallel to each other, indicating a constant ratio of the critical Grashof numbers between the constant property and variable viscosity cases, approximately equal to 1.48. The average wavenumbers of the secondary cells at the onset are provided in Table 1. They are larger than the experimental results by Chen and Thangam [5], with better agreement for the higher concentration fluid.

The viscosity ratio, ν_c/ν_h, at the onset of the secondary flow is shown in Table 1. It is very small at $C = 70\%$ case, equal to 2.16, and increases rapidly with the glycerine concentration, reaching 29.5 at $C = 90\%$. The nondimensional vertical temperature gradients S_1 and S_2 obtained just before the onset of the secondary flow are presented in Table 1. Here S_1 is calculated based on the temperatures at the points adjacent to the center, and S_2 based on the temperatures at the locations $y = 0.25$ and 0.75 at the central line. We find S_1 may be disturbed by the slightly wavelike variation of the temperature at the central zone. We obtain $S_1 = 0.388$, 0.328 and 0.304 and $S_2 = 0.479$, 0.463 and 0.430 for $C = 70$, 80 and 90%, respectively. The values of S_1, except at $C = 70\%$, are in good agreement with the corresponding experimental results by Chen and Thangam [5], who presented a mean value of 0.315 for all of the cases. The values of S_2 are larger than S_1, and smaller than the experimental results by Elder [1], who obtained a value of 0.55 for 100 cSt silicone oil and 0.50 for paraffin based on the temperatures at $y = 0.4$ and 0.6. Considering the effect of viscosity variation, Elder [1] gave the following correlation to the vertical temperature gradients

$$S = 0.50\left(1 - 0.04\left(\frac{\nu_m}{\nu_h} - 1\right)\right). \tag{12}$$

Substituting the values of ν_h/ν_m, shown in Table 1, at the onset of the secondary flow, we obtain $S = 0.491$, 0.474 and 0.443, very close to our results of $S_2 = 0.479$, 0.463 and 0.430, respectively.

4.3. *Heat transfer results*

The local heat transfer rate along any vertical plane in the slot is given by

$$Nu_L = -\partial\theta/\partial x + PrGru\theta. \tag{13}$$

Its variation along the hot wall is similar to that of the constant viscosity fluid. The average heat transfer rate is calculated by the Simpson's rule, and is shown

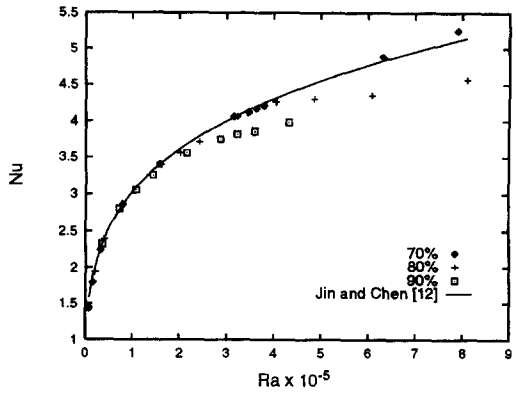

Fig. 7. Variation of average Nusselt numbers with the Rayleigh number.

in Fig. 7. The result for constant viscosity fluid case is also shown. We find, for $C = 70\%$ the heat transfer rate is independent of the Prandtl number, and is almost the same as that of the constant viscosity fluid. For solutions of higher glycerine concentration, the heat transfer rate is the same as that for the constant viscosity fluid at low Rayleigh numbers but becomes lower at higher Rayleigh numbers. This result is qualitatively in agreement with the experiments of Seki *et al.* [9], who found that the heat transfer rate varies slightly with the Prandtl number.

Considering the effect of variable viscosity on heat transfer, we can modify the correlation given by Jin and Chen [15] for the constant property fluid in the following form

$$Nu = 0.1631 Ra^{0.2537}/\delta(\nu_h/\nu_m) \tag{14}$$

where

$$\delta(\nu_h/\nu_m) = \max\{1, 1.210 - 0.4776\nu_h/\nu_m\}$$

is the effect of the variable viscosity, and ν_h/ν_m is the ratio of viscosities at the hot wall temperature and the mean temperature.

5. CONCLUSIONS

Natural convection of high Prandtl number fluids with variable viscosity, 70, 80 and 90% glycerine–water solutions, in a vertical slot of aspect ratio 15 has been studied numerically by solving the fully nonlinear governing equations. The four-parameter fit by Chen and Pearlstein [8] is adopted to calculate the variation of viscosity with temperature. The flow patterns and the critical Grashof numbers at the onset of the convective instability predicted in this study are in good agreement with the experimental results by Chen and Thangam [5]. The critical Grashof number is smaller than the corresponding value for the constant property fluid due to the variation of the fluid viscosity. The vertical temperature gradient is smaller than that in the constant property case, and decreases slightly as the glycerine concentration increases. We confirm that the flow is non-symmetric. The upward boundary layer becomes thinner while the downward boundary layer becomes thicker as the viscosity variation increases. The secondary cells at the onset appear in the upper portion of the central core only due to viscosity stratification and the stabilizing effect of larger vertical temperature gradient in the lower region. Similarly, the large horizontal temperature gradient near the cold wall displaces the secondary cells towards the hot wall. The heat transfer rate is slightly smaller than that in constant property case as the viscosity variation becomes large.

Acknowledgements—The financial support of NASA Microgravity Science and Application Division through grant NAG 3-1386 is gratefully acknowledged.

REFERENCES

1. J. W. Elder, Laminar free convection in a vertical slot, *J. Fluid Mech.* **23,** 77–98 (1965).
2. C. M. Vest and V. S. Arpaci, Stability of natural convection in a vertical slot, *J. Fluid Mech.* **36,** 1–15 (1969).
3. J. E. Hart, Stability of the flow in a differentially heated box, *J. Fluid Mech.* **47,** 547–576 (1971).
4. Y. Lee and A. Korpela, Multicellular natural convection in a vertical slot, *J. Fluid Mech.* **126,** 91–121 (1983).
5. C. F. Chen and S. Thangam, Convective stability of a variable-viscosity fluid in a vertical slot, *J. Fluid Mech.* **161,** 161–173 (1985).
6. S. Thangam and C. F. Chen, Stability analysis on the convection of a variable viscosity fluid in an infinite vertical slot, *Phys. Fluids* **29,** 1367–1372 (1986).
7. Y.-M. Chen and A. J. Pearlstein, Stability of free-convection flows of variable-viscosity fluids in vertical and inclined slots, *J. Fluid Mech.* **198,** 513–541 (1989).
8. Y.-M. Chen and A. J. Pearlstein, Viscosity–temperature correlation for glycerol–water solutions, *Ind. Engng Chem. Res.* **26,** 1670–1672 (1987).
9. N. Seki, S. Fukusako and H. Inaba, Visual observation of natural convection flows in a narrow vertical cavity, *J. Fluid Mech.* **84,** 695–704 (1978).
10. F. L. Chen and C. H. Wu, Unsteady convective flows in a vertical slot containing variable viscosity fluids, *Int. J. Heat Mass Transfer* **36,** 4233–4246 (1993).
11. S. Wakitani Experiments on convective instability of large Prandtl number fluids in a vertical slot, *ASME J. Heat Transfer* **116,** 120–126 (1994).
12. P. J. Roache, *Computational Fluid Dynamics*. Hermosa, Albuquerque, NM (1982).
13. J. P. Van Doormaal and G. D. Raithby, Enhancement of the SIMPLE method for predicting incompressible fluid flows, *Numer. Heat Transfer* **7,** 147–163 (1984).
14. S. V. Patankar, A calculation procedure for two-dimensional elliptic situations, *Numer. Heat Transfer* **4,** 409–425 (1981).
15. Y. Y. Jin and C. F. Chen, Instability of convection and heat transfer of high Prandtl number fluids in a vertical slot, *ASME J. Heat Transfer* **118** (1996).
16. P. Le Quéré, A note on multiple and unsteady solutions in two-dimensional convection in a tall cavity, *ASME J. Heat Transfer* **112,** 965–974 (1990).
17. G. Lauriat and G. Desrayaud, Natural convection in air-filled cavities of high aspect ratios : discrepancies between experimental and theoretical results, ASME Paper 85-HT-37 (1985).